Sustainable Horizons 13 (2025) 100125

Contents lists available at ScienceDirect

Sustainable Horizons

journal homepage: www.elsevier.com/locate/horiz

Original Research Articles

Power performance and dynamic characteristics of a 15 MW floating wind turbine with wave energy converter combined concept

Xun Gu [a], Fei Lin [b], Wei Jiang [b], Jie Xu [a], Jia-Ming Liu [c], Kai Wang [c,*], Tao Tao [d]

[a] Guangdong Datang International Chaozhou Power Generation Co., Ltd., Chaozhou 515700, China
[b] China Datang Corporation Ltd. Guangdong Branch, Guangzhou 510000, China
[c] School of Ocean Engineering and Technology, Sun Yat-sen University, & Southern Marine Science and Engineering Guangdong Laboratory (Zhuhai), Zhuhai, 519082, China
[d] China Southern Power Grid Technology Co, Ltd, Guangzhou 510080, China

ARTICLE INFO

Keywords:
Floating offshore wind turbine
Wave energy converter
Combined concept
Power performance
Dynamic response
Semi-submersible

ABSTRACT

Recently, the large-scale development of Floating Offshore Wind Turbines (FOWTs) has raised attention to efficient energy capture and conversion. Combining a wave energy generator with a wind turbine system enhances the overall power production and reduces operating costs, effectively lowering the Levelized Cost of Electricity (LCoE). This work proposes a novel combined wind-wave energy generation concept consisting of a 15 MW class semi-submersible FOWT and four heaving-type torus-shape Wave Energy Converters (WECs) integrated with the platform columns. A fully coupled numerical model of aero-hydro-elastic-servo-mooring is developed based on the SIMO-RIFLEX framework. The power performance and dynamic response of the combined concept are statistically and analytically investigated by time-domain simulation for several sets of working load cases. The results show that introducing tori will bring additional restoring moments and damping effects to the platform, contributing to stable motion. In the rated operating condition, the pitch amplitude of the combined concept is 31.5 % less than that of the FOWT. At the same time, the torus-shaped WECs hardly affect the power performance of the wind turbine. The combined concept provides an additional contribution of wave energy, which is about 11.4 % of the annual power production in the rated operating case. Regarding dynamic characteristics, the combined concept exhibits a greater sensitivity to wave excitation.

1. Introduction

Offshore wind is the most significant climate mitigation opportunity in the oceans (GWEC, 2024). A Floating Offshore Wind Turbine (FOWT) is prioritized over a fixed wind turbine in water depths greater than 50 m due to its economic advantages (Musial et al., 2006). However, the expensive floating platform and mooring system still lead to a very high Cost of Energy (CoE). Meanwhile, the non-fixed platform introduces more intense motions and loads to the whole system, increasing the risk of structural failure and shortening the service life. Besides the optimization of system components (Hegseth et al., 2020; Xu et al., 2021a,b) and control strategies (Namik and Stol, 2014; Si et al., 2014; Creech et al., 2015), the combination of floating platforms with Wave Energy Converter (WEC) was found to be a potential solution to reduce the motion response and structural loads of FOWTs effectively. On the one hand, the FOWT, as the major part, allows the sharing of the platform, mooring system, electric cables, and other components with WEC, which reduces the construction and operational costs; on the other hand, the introduction of WEC increases the power capacity, contributing to a further reduction in the Levelized CoE of the FOWT system. In addition, the enhanced local wave height due to the diffraction and radiation from the platform would also promote the power performance of WECs (Zhou et al., 2023). Therefore, combining FOWT with WECs has been widely regarded as a promising solution for improving its power gain and load behavior (Astariz et al., 2016).

Recently, a series of interesting combined concepts of FOWT and ocean energy converters have been proposed (Hu et al., 2020; Yang et al., 2020; Sun et al., 2021; Zhang et al., 2022). In these designs, it is essential to ensure that the adverse impacts of WECs on the existing platform are effectively mitigated, optimizing space utilization,

* Corresponding author.
E-mail addresses: 958414778@qq.com (X. Gu), 1006334078@qq.com (F. Lin), jiangwei_cdt@126.com (W. Jiang), 361905557@qq.com (J. Xu), liujm87@mail2.sysu.edu.cn (J.-M. Liu), wangkai25@mail.sysu.edu.cn (K. Wang), taot0804@163.com (T. Tao).

https://doi.org/10.1016/j.horiz.2024.100125
Received 24 July 2024; Received in revised form 15 September 2024; Accepted 12 October 2024
Available online 11 November 2024

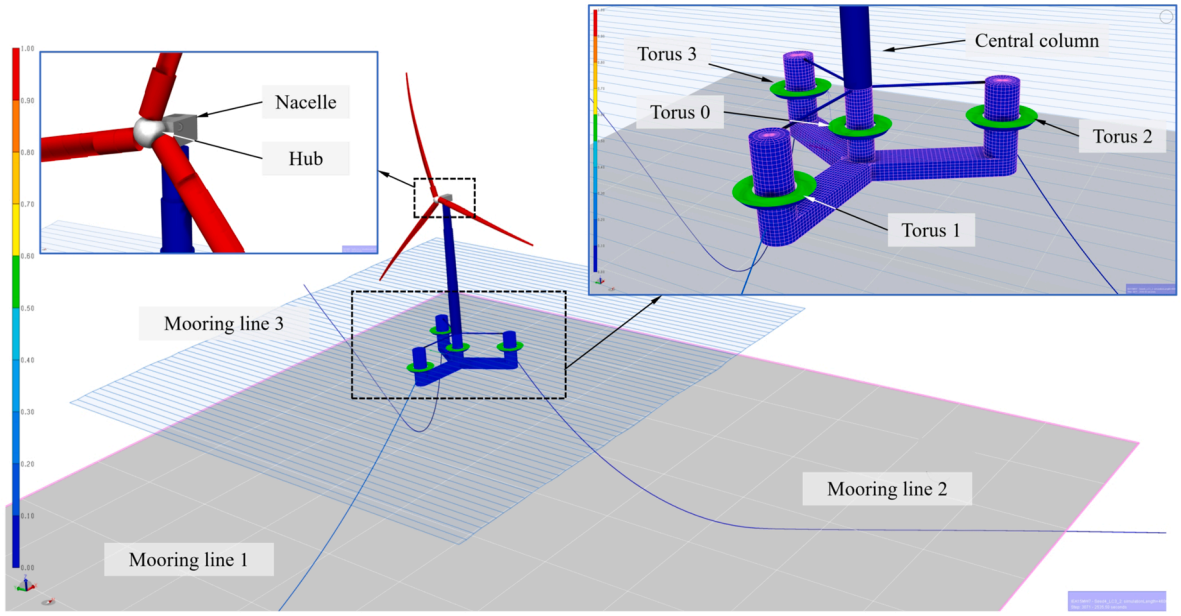

Fig. 1. Diagram of the combined concept.

minimizing construction complexity, and pursuing cost-effective solutions. Several typical concepts are proposed by the European project (MARINA Platform, 2014), including solutions based on Oscillating Water Column (OWC) (Aubault et al., 2011; Peiffer et al., 2011, 2012), the Semi-submersible Flap Combination (SFC) (Michailides et al., 2016a,b), and the Spar Torus Combination (STC) (Muliawan et al., 2012, 2013a,b). Peiffer et al. (2011) integrated a power device named Spherical Wave-Energy DEvice (SWEDE) into Windfloat. They found that SWEDE achieves the maximum average mechanical power in waves with a period of 6 s, which can be fulfilled in most of the ocean. Aubault et al. (2011) accurately simulated the power production of the Windfloat with an OWC WEC system by using the diffraction-radiation code WAMIT and PTO assumption, proving that the installation of a WEC is effective in reducing the project's economic costs. A combined DeepCwind-OWC concept was proposed by Zhang et al. (2022), and the results showed that the Power Take-off (PTO) gain-scheduling control scheme could mitigate the pitch response of the platform and tower base fatigue loads. The SFC concept comprises a semi-submersible platform and several fully submersible flap-type WECs. The results of (Michailides et al., 2016a) show that the SFC absorbs objective wave energy while the flap-type WEC causes a little effect on the mooring tension, motion dynamics, and tower-base bending moment. Recently, Hu et al. (2020) proposed a hybrid system combining a heaving WEC array and Windfloat and showed that the WEC array can reduce the pitch response of the platform. Further, Zhou et al. (2023) analyzed the effect of the number and size of floats on motion response and power performance of the hybrid system. Si et al. (2021) installed a point-absorber type WEC named Wavestar on the outside of each offset column of the OC4-DeepCwind platform. They revealed the significant effect of PTO on power production and dynamic performance. Similarly, Kamarlouei et al. (2020) investigated the effect of the PTO control strategy on the WEC array via model test.

Another representative concept for wind-wave energy combination is STC, which consists of a spar-type FOWT with a torus WEC. Muliawan et al. (2012, 2013a,b) demonstrated that the STC system has better motion response and more stable power output than the original spar wind turbine. There is always a positive synergy between the platform and the floats in operating conditions. However, it is a challenge to maintain the structural integrity under extreme wind and wave conditions. Therefore, Ren et al. (2014, 2015) investigated the long-term performance of the STC system in terms of annual power production, structural fatigue damage, and extreme response under different survival modes. In addition, Wan et al. (2015, 2016b) successively analyzed the response characteristics of the STC system in extreme and typical operating sea states and reproduced the response under two strategies in experiments. Wan et al. (2014, 2016a) discussed the strong nonlinear effects, such as the slamming and the green water, that may occur in torus WECs under normal and extreme states. Cheng et al. (2019) combined a torus WEC with a spar Vertical Axis Wind Turbine (VAWT) based on the STC concept and investigated the effect of WEC on dynamic response and power performance. Similarly, a novel concept combining a WEC with a TLP platform was proposed by Ren et al. (2020), proving that the concept can effectively mitigate the horizontal motion response via numerical calculations and a 1:50 scaling test.

Among all FOWT platforms, the semi-submersible type has excellent potential due to its wide water depth range, ease of installation and maintenance, and low construction and modification difficulties. Recently, several studies have focused on integrating STC with semi-submersible platforms. Li et al. (2021) investigated the dynamic response, power production, and mooring tension of a hybrid system that uses the 5-MW-CSC platform (Luan et al., 2016) with a torus WEC on the central column. Another interesting work was conducted on the same platform, with the difference that the new concept was equipped with a torus-type WEC for each column to enhance the wave energy harvesting capability (Li et al., 2022). Tian et al. (2023) compared the impact of different numbers of WECs on the produced power of the combined structure.

All the concepts above are considered positive conclusions, especially regarding power performance. However, to the author's best knowledge, most of the existing works have been performed based on the 5 MW class wind turbine. In recent years, the wind turbine power capacity scale has increased, with units between 8 and 12 MW becoming the norm. Up to now, data for high-power wind turbines such as DTU 10 MW (Bak et al., 2013), IEA 15 MW (Gaertner et al., 2020), and IEA 22 MW (Zahle et al., 2024) have been open-sourced, making it possible to study high-power turbines. Motivating factors for the relevant research are as follows: one is that FOWT is subjected to more intense and complex environmental loads due to the large structures and flexible materials, and the other is that the additional WEC introduces unknown effects to the original system. Therefore, we investigate the dynamic

Table 1
Main parameters of the semi-submersible FOWT.

Component	Parameter	Unit	Value
Platform	Hull displacement	[m^3]	20,206
	Mass	[t]	17,839
	Draft	[m]	20
	Freeboard	[m]	15
	Vertical center of Gravity (CoG) from SWL	[m]	–14.94
	Vertical center of Buoyancy (CoB) from SWL	[m]	–13.63
	Operating water depth	[m]	200
Wind turbine	Rating	[MW]	15
	Cut-in, rated, cut-out wind speed	[m/s]	3, 10.59, 25
	Minimum, rated rotor speed	[rpm]	5, 7.55
	Blade length	[m]	120
	Max chord	[m]	5.77
	Hub height from SWL	[m]	150
	Rotor Nacelle Assembly (RNA) mass	[t]	991
	Tower mass	[t]	1263 (1249.59)
	Tower length	[m]	129.495
Mooring system	Type	[–]	Chain catenary
	Number of lines	[–]	3
	Line length (unstretched)	[m]	850
	Anchor depth	[m]	200
	Fairlead depth	[m]	14
	Fairlead radial spacing	[m]	58
	Dry line linear density	[kg/m]	685
	Nominal chain diameter	[mm]	185

Table 2
Main parameters and properties of the torus.

Parameter	Unit	Value	
		Torus #0	Torus #1, 2, & 3
Outer diameter at the SWL	[m]	24	26
Inner diameter at the SWL	[m]	12	14
Mass	[t]	4.7956E+05	5.1145E+05
Height	[m]	8	8
Draft	[m]	2	2
COG from SWL	[m]	–0.9	–0.9
Stroke length	[m]	6	6
Stiffness upper end stop spring	[kN/m]	1E+06	1E+06
Stiffness lower end stop spring	[kN/m]	1E+06	1E+06
PTO damping coefficient	[kN·s/m]	2000, 8000, 12,000	2000, 8000, 12,000
PTO stiffness coefficient	[kN/m]	10	10

response and power performance of a 15 MW semi-submersible FOWT with four torus-type WECs novel combined system. In this work, a platform named UMaine VolturnUS-S (Allen et al., 2020) that supports the IEA 15 MW turbine was adopted, and the free decay test was conducted as a pilot study. Next, the WECs were added to the columns to compare the effect of PTO on power production. Finally, we discussed the effects of WECs on the aerodynamics, floater motion, tower bending moment, and mooring tension of the concept.

The rest of this paper is organized as follows. Section 2 describes the main parameters of the combined concept in detail. Section 3 introduces the aero-hydro-elastic-servo-mooring coupled framework and methodology. Section 4 shows the selection and results of the loading cases. Section 5 focuses on the dynamic response and power performance of the concept. Section 6 organizes the main conclusions, limitations, and outlook.

2. Description of the combined FOWT-WEC concept

The wind-wave energy converter proposed in this study is shown in Fig. 1. This combined concept comprises a Horizontal Axis Wind Turbine (HAWT), a semi-submersible support platform, a mooring system, and four WECs. The layout of the WECs is inspired by Li et al. (2022), which combines the ideas of SFC and STC by equipping a torus-type point-absorber WEC on each column of the platform. While the turbine works, the WECs are in a relative heave motion with the platform slide along the columns, forcing the hydraulic power generators to convert the wave energy into electrical energy. A detailed description of the combined concept is given in the following subsections.

2.1. Semi-submersible FOWT

The FOWT system used in this work is UMaine VolturnUS-S. In this case, the IEA-15–240-RWT reference wind turbine released by the National Renewable Energy Laboratory (NREL) is mounted on the central column, and three radial columns are connected to the anchors via a three-line catenary mooring array to add yaw stiffness. The design of the semi-submersible turbine needed to be modified from the IEA 15 MW fixed turbine. The main parameters of the FOWT are listed in Table 1, and a detailed description can be found in (Allen et al., 2020). Note that the values in parentheses (if any) are taken from our model due to minor differences in modeling methods.

2.2. Torus-shaped WEC

The torus pushes the piston by relative heave sliding with the column, forcing the pressurized fluid in the hydraulic cylinder to drive the generator to realize the wave energy-electricity conversion. Fig. 1 shows the diagram of the combined system, where each WEC is distributed geometrically concentric with the corresponding column, respectively. The main parameters and properties of torus are listed in Table 2. Note that the central WEC has a smaller inner and outer diameter than the others because of the different cross-sections of the corresponding column.

3. Methodology

In this work, the fully coupled aero-hydro-elastic-servo-mooring time domain simulation of the FOWT-WEC concept is realized via the SIMO-RIFLEX code. In particular, the SIMO solver is used to compute the hydrodynamic loads and motions of rigid bodies such as platforms and WECs. In contrast, RIFLEX is a flexible-body nonlinear finite-element solver calling SIMO to realize coupling. Both are developed by SINTEF Ocean and are widely used in the offshore oil and gas industries and other marine operations (Cheng et al., 2017). The wind turbine controller is adjusted based on the NREL Reference Open Source Controller (ROSCO) version 2.9.0 with minor adaptations to account for floating platform dynamics (IEA, 2024).

3.1. Hydrodynamics

The hydrodynamic coefficients of the platform and the torus-type WECs, i.e., the added mass, potential damping, and first-order excitation force are estimated by the HydroD based on the frequency-domain boundary element method. Then, the relevant results are imported into SIMA to carry out the coupling calculations in the time domain. The viscous forces on the platform and tori can be estimated using Morison's drag formula:

$$F_D = \frac{1}{2}\rho_w C_D D(u-\dot{\eta})|u-\dot{\eta}| \quad (1)$$

where the seawater density ρ_w is taken as 1.03×10^3 kg/m^3; C_D is the

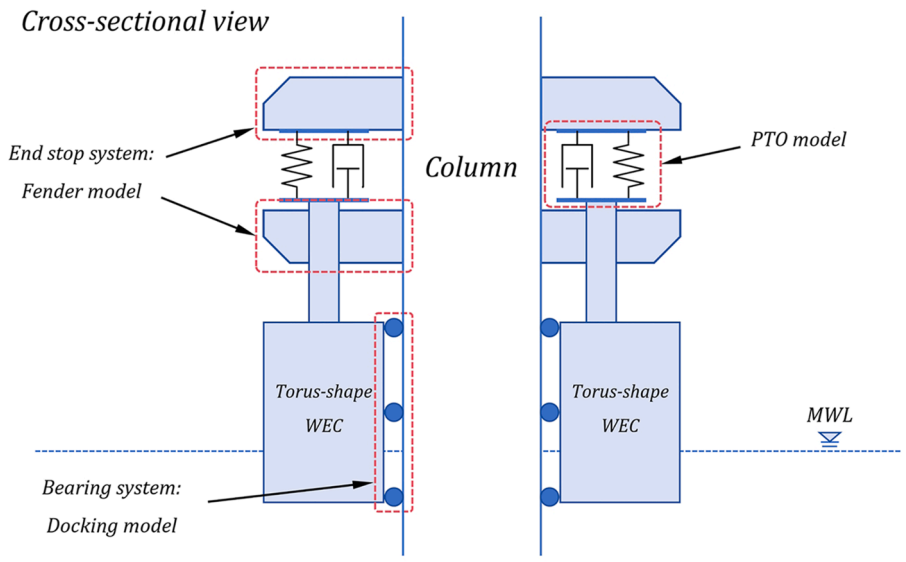

Fig. 2. Diagram of the mechanical constraints between WEC and platform column.

Table 3
Load cases.

Load case	Wind load		Irregular wave load			Remark
	U_w [m/s]	T_I [–]	H_s [m]	T_p [s]	γ_p [–]	
LC-1	3.00	0.314	1.82	9.73	3.3	Cut-in
LC-2	6.00	0.202	2.17	9.75	3.3	–
LC-3	10.59	0.153	2.83	9.96	3.3	Rated
LC-4	15.00	0.135	3.57	10.27	3.3	–
LC-5	20.00	0.124	4.50	10.69	3.3	–
LC-6	25.00	0.117	5.53	11.15	3.3	Cut-out

Table 4
Natural periods.

Direction	Value			
	VolturnUS-S (Allen et al., 2020) [s]	FOWT system in present work [s]	Relative error [%]	Combined concept in present work [s]
Surge	142.9	136.6	–4.36	143.3
Sway	142.9	136.9	–4.19	144.7
Heave	20.4	20.6	0.98	13.5
Roll	27.8	29.3	5.47	14.8
Pitch	27.8	29.4	5.73	14.7
Yaw	90.9	90.1	–0.85	97.0

drag coefficient; D is the projected area; and u and $\dot{\eta}$ are the velocities of the water particle and the rigid body, respectively.

3.2. Aerodynamics

The aerodynamic loads on the blades are calculated by using the Blade Element Momentum (BEM) theory. Each blade is discretized into infinite two-dimensional airfoil-shaped micro-elements along the airfoil spread direction with independence for fluid motion. Thus, the thrust and torque on the whole blades are obtained by integrating the forces and moments on these blade elements:

$$\mathrm{d}T = \mathrm{d}L\cos\varphi + \mathrm{d}D\sin\varphi = \frac{1}{2}N\rho_a U^2(C_l\cos\varphi + C_d\sin\varphi)c\mathrm{d}r \tag{2}$$

$$\mathrm{d}Q = \mathrm{d}L\sin\varphi - \mathrm{d}D\cos\varphi = \frac{1}{2}N\rho_a U^2(C_l\sin\varphi - C_d\cos\varphi)cr\mathrm{d}r \tag{3}$$

where $\mathrm{d}T$, $\mathrm{d}Q$, $\mathrm{d}L$, and $\mathrm{d}D$ are the thrust, torque, lift, and drag forces on the blade element, respectively; the number of blades N is taken as 3 in this case; C_l and C_d are the lift and drag coefficients, respectively; the air density ρ_a is taken as 1.29 kg/m^3; φ is the incidence angle; U is the incoming airflow velocity; c is the chord length of the airfoil; and r is the distance between the blade element and the hub. We also adopt a series of optimization methods to correct the defects in the original model, such as Prandtl tip loss correction, hub loss correction, and Glauert correction at large-induced velocities.

3.3. Structural dynamics

The semi-submersible platform and torus-type WECs are considered as rigid bodies, the wind turbine blades and tower are represented by nonlinear beam elements, and the mooring lines are modeled by nonlinear bar elements.

3.4. Mechanical coupling dynamics

Only relative heave motion exists between the platform and the WEC, while the rest of the five Degrees of Freedom (DoFs) are constrained by the bearing system (horizontal limiter) and the end stop system (vertical limiter), as shown in Fig. 2. The bearings are simulated in a set of spring-damping combinations by the docking model, where the column and the WEC are considered as a guide pin and a docking cone, respectively. Hence, when a relative motion occurs between the two in the horizontal plane, the docking model provides radial contact forces to dampen the motion. The end stop system is replaced by the fender model, which restricts the motion range of the WECs by monitoring the distance between the WEC and the fender model and applying a variable force. Here, the maximum relative vertical stroke is set to ±3 m. Detailed modeling can be found in Muliawan et al. (2011, 2013b).

3.5. PTO model

The PTO system described in this subsection is a part of WEC. Here, the PTO model is equivalently simplified as combining a linear damping with B_{PTO} and a linear spring with K_{PTO}. The internal force F generated by this combination in the hybrid concept can be expressed as:

$$F = F_B + F_K = B_{PTO}\dot{\eta}_r + K_{PTO}\eta_r \tag{4}$$

where η_r is the relative heave motion between the platform and the torus

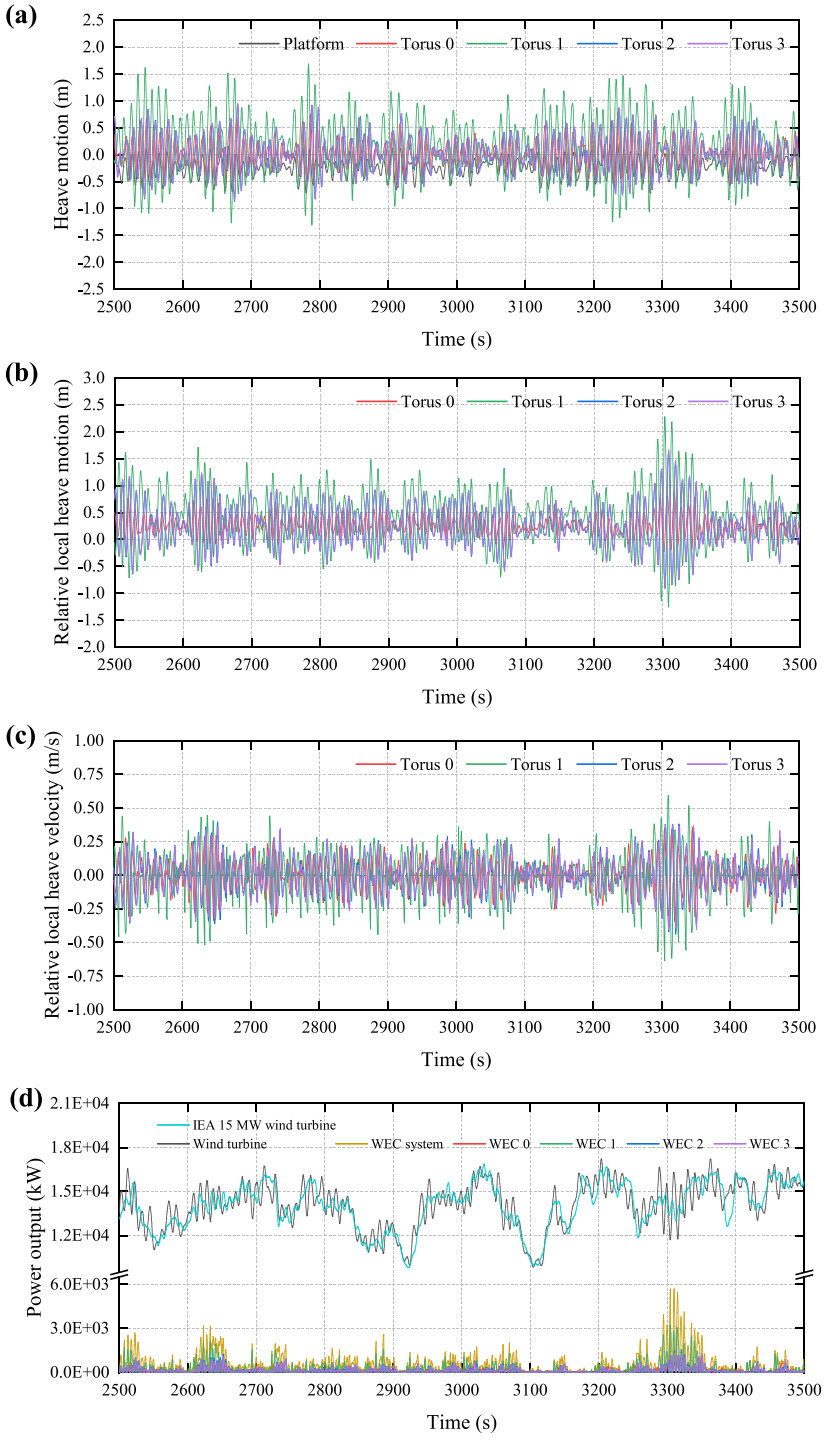

Fig. 3. Coupled motion and power output: (a) heave motion, (b) relative heave motion, (c) relative heave velocity, and (d) power output.

WEC; F_B and F_K denote the damping and spring contributions, which are proportional to the relative heave velocity and motion, respectively. Additionally, the WEC output power is related to the damping coefficient B_{PTO} and the relative motion η_{r}:

$$P_{\mathrm{WEC}} = F_B\dot{\eta}_{\mathrm{r}} = B_{\mathrm{PTO}}\dot{\eta}_{\mathrm{r}}^2 \tag{5}$$

As we can see, the larger the damping coefficient B_{PTO} and relative motion η_{r}, the more wave energy the WEC absorbs in this model.

4. Environmental conditions and load cases

This study only evaluates the power performance and dynamic response of the combined concept under operating sea states, so no shutdown occurs for the turbine. In addition, the load cases (LCs) combine a series of turbulent wind and irregular waves, and the wind and waves all propagate positively along the *x*-axis.

Turbulent wind fields are generated using the TurbSim code (Jonkman., 2009) based on the Kaimal wind spectrum defined in the international standard IEC 61,400–1 Class C (IEC, 2005). Wind profiles using the Normal Turbulence Model (NTM) from the standard. Taking

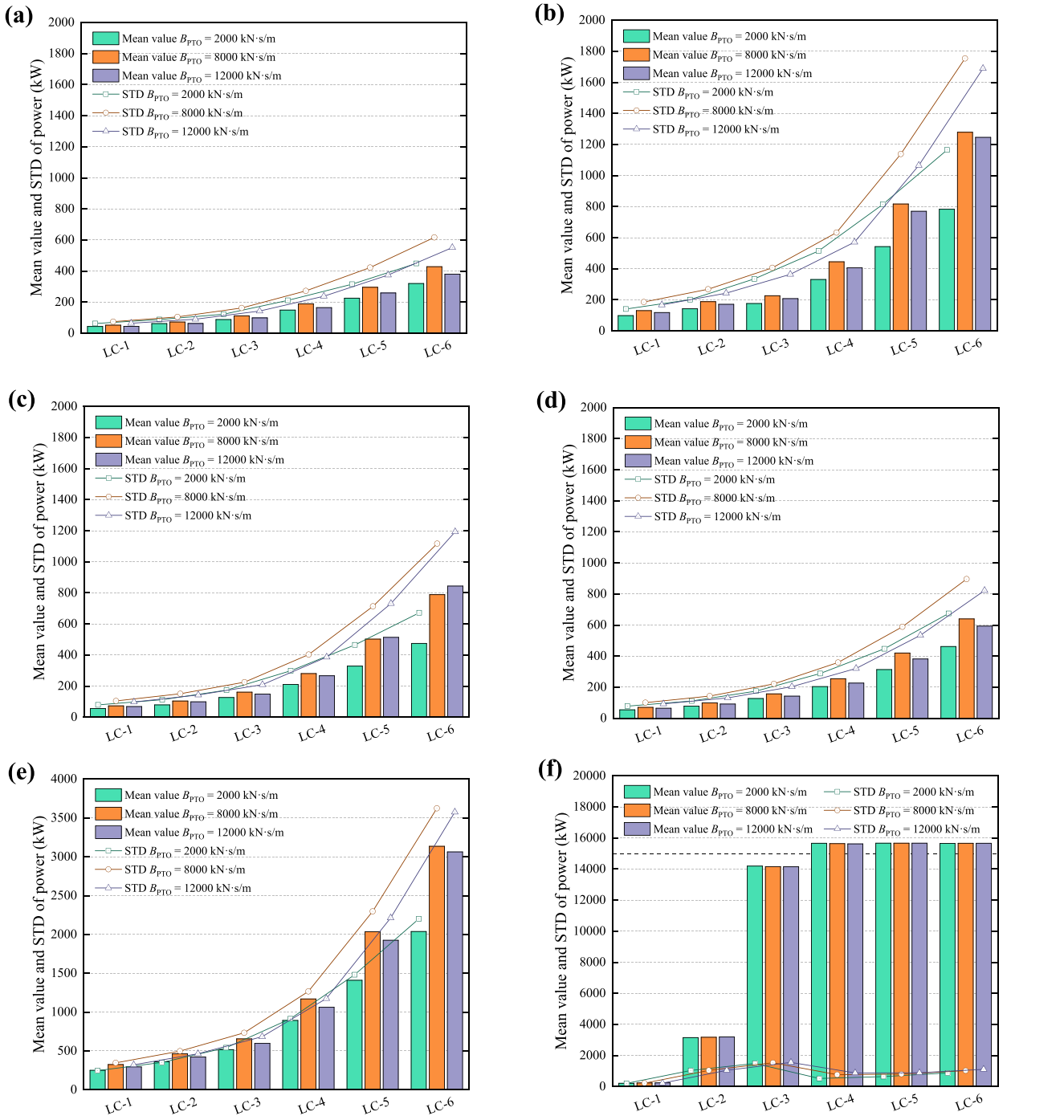

Fig. 4. Mean values and STDs of 1-h wind and wave power output of the combined system in different LCs: (a) WEC 0, (b) WEC 1, (c) WEC 2, (d) WEC 3, (e) WEC system, and (f) wind turbine.

into account the roughness of the sea surface, the average wind speed at height z above the Mean Sea Level (MSL) can be expressed in the form of power law:

$$U(z) = U_{\text{ref}}\left(\frac{z}{z_{\text{ref}}}\right)^{\alpha} \tag{6}$$

where U_{ref} is the reference wind speed at a reference height z_{ref} above the MSL, z_{ref} in this work equals to the hub height 150 m; α is taken as 0.14. The wave field is generated based on the JONSWAP spectrum by giving the significant wave height H_s and the spectral peak period T_p.

The wind-wave conditions in this study are referenced to data from the Statfjord site in the northern North Sea. The density function of wind-wave joint distribution in this area was expressed as the product of a marginal distribution and a conditional distribution by Johannessen et al. (2002):

$$f_{U_{10}H_sT_p}(u_{10},h_s,t_p) = f_{U_{10}}(u_{10})\cdot f_{H_s|U_{10}}(h_s|u_{10})\cdot f_{T_p|H_sU_{10}}(t_p|h_s,u_{10}) \tag{7}$$

where u_{10} is the 1-h average wind speed at 10 m above the MSL.

The marginal distribution of U_{10} corresponds to a two-parameter Weibull distribution:

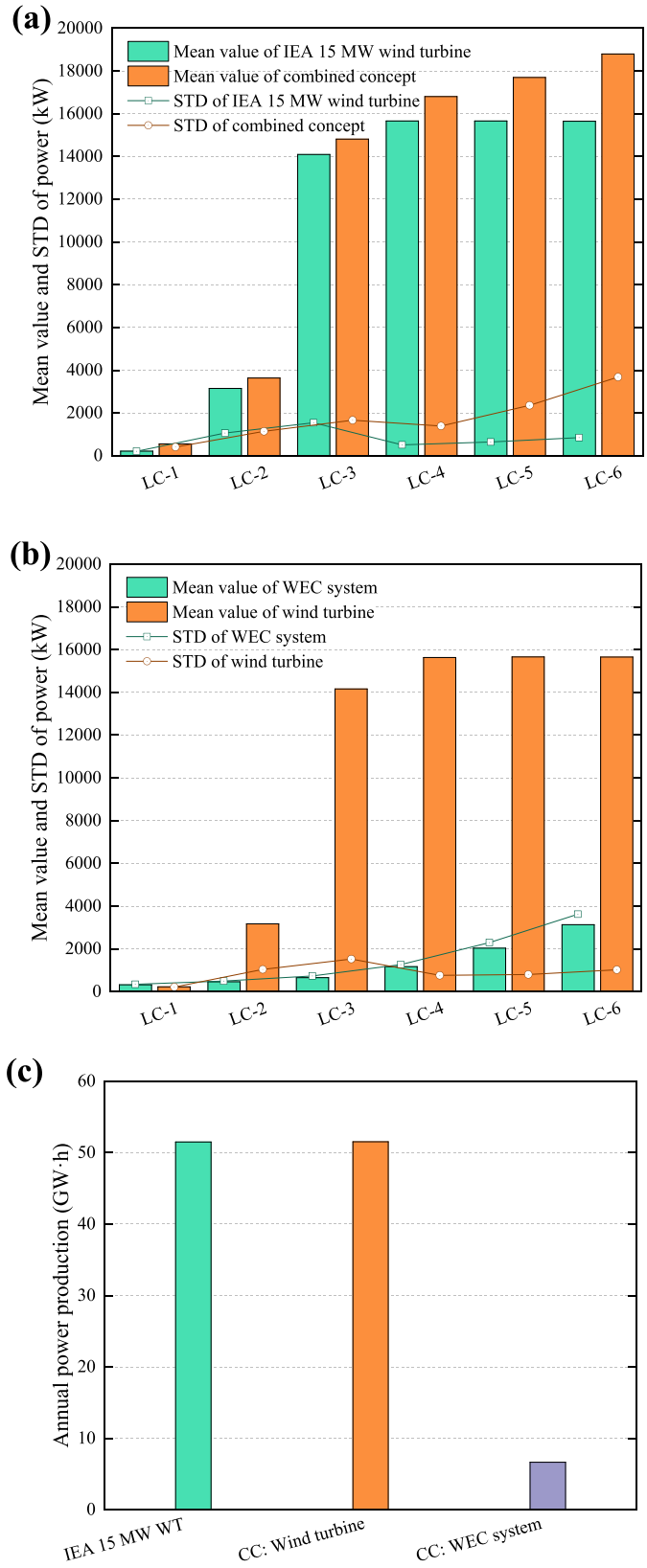

Fig. 5. Statistical comparisons of wind and wave power performance: (a) IEA 15 MW wind turbine versus combined concept, (b) WEC system versus wind turbine, and (c) annual power production.

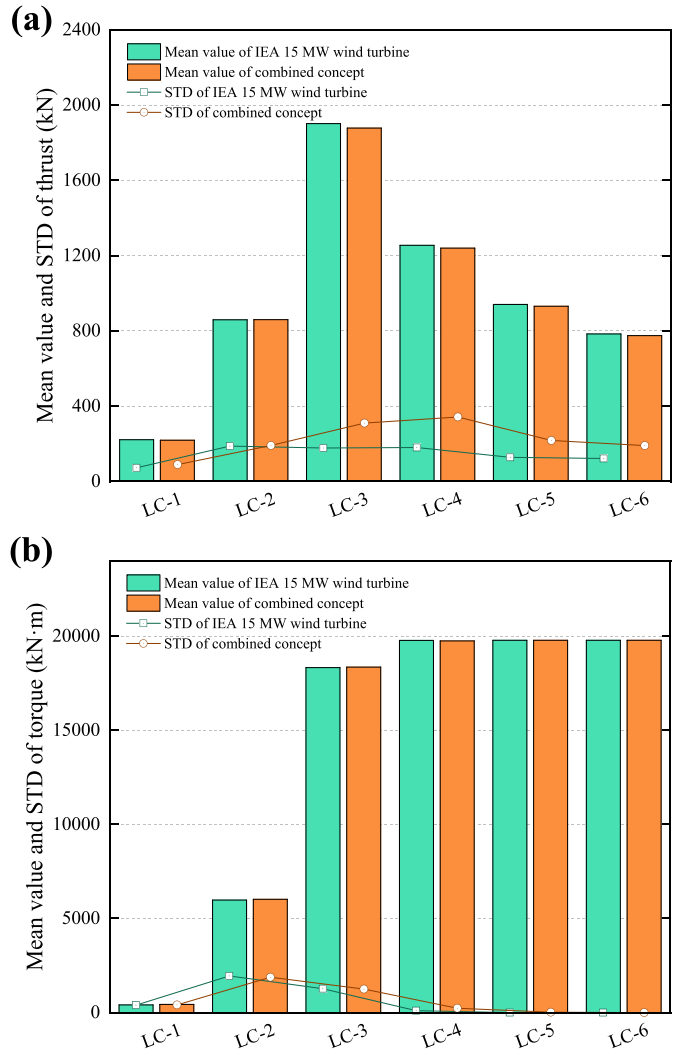

Fig. 6. Statistical comparisons of thrust and torque in combined concept and IEA 15 MW wind turbine: (a) thrust and (b) torque.

$$f_{U_{10}}(u_{10}) = 1 - \exp\left\{-\left(\frac{u_{10}}{\beta_1}\right)^{\alpha_1}\right\} \tag{8}$$

where the shape parameter α_1 and scale parameter β_1 are taken as 1.708 and 8.426, respectively.

The conditional distribution of H_s also follows a two-parameter Weibull distribution, and the expression is the same as Eq. (8). For a given U_{10}, the expected value of the significant wave height H_s is:

$$E(H_s) = \beta_2 \Gamma\left(\frac{1}{\alpha_2} + 1\right) \tag{9}$$

where the shape parameter α_2 is taken as $2 + 0.135u_{10}$; the scale parameter β_2 is taken as $1.8 + 0.1u_{10}^{1.322}$.

The conditional distribution of T_p follows a log-normal distribution. For a given U_{10} and H_s, the expected value of the spectrum peak period T_p is:

$$E(T_p) = (4.883 + 2.68h_s^{0.529})\left\{1 - 0.19\left(\frac{u_{10} - (1.764 + 3.426h_s^{0.78})}{1.764 + 3.426h_s^{0.78}}\right)\right\} \tag{10}$$

For given wind speeds, a series of wind-wave LCs can be obtained by applying Eqs. (6), (9), and (10), as listed in Table 3. Where U_w is the wind speed at the reference height, i.e., U_{ref} in Eq. (6), and the spectral

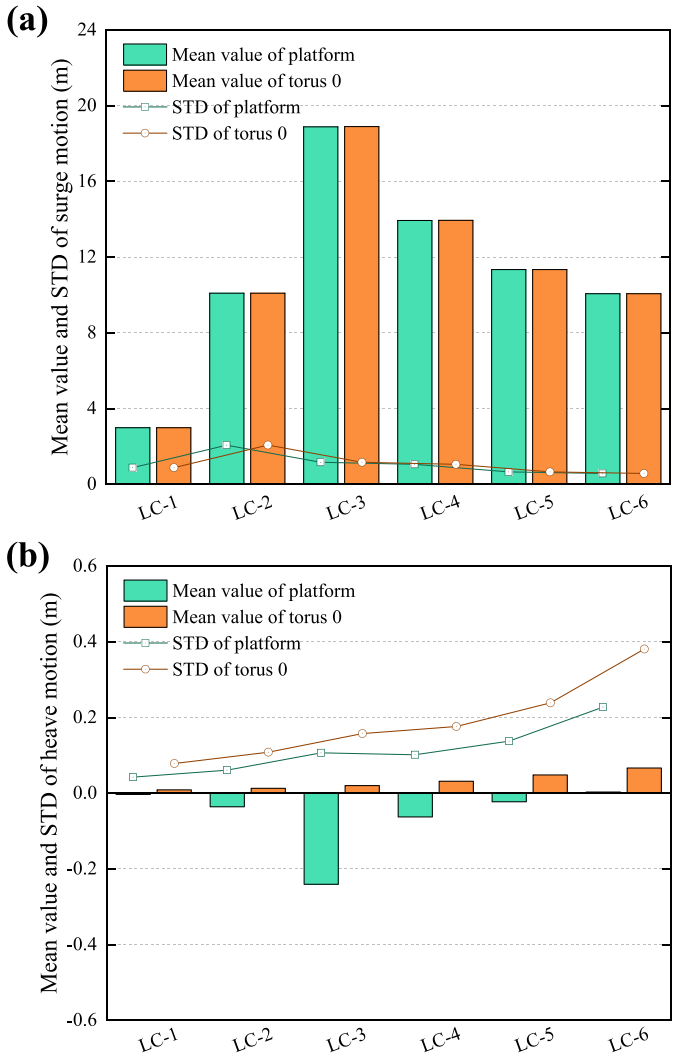

Fig. 7. Statistical comparisons of surge and heave motions of the platform and torus 0 in the combined concept: (a) surge motion and (b) heave motion.

peak factor γ_p is set as 3.3. Each set of LCs is simulated for 4600 s, of which the first 1000 s are neglected to eliminate the initial transient effect, resulting in 1-h data. The statistical analysis in Section 5 is conducted based on the average values of five random wave simulation results. In contrast, the wind fields are the same in each set of LCs due to the limited effect on WEC power generation efficiency.

5. Results and discussion

5.1. Free decay test

Free decay tests are conducted in calm water without wind and wave loads to ensure the reliability of the model. Table 4 lists the natural periods of 6-DoFs of the relevant systems. The natural period of the FOWT model in this study remains within 10 % of the relative error with VolturnUS-S platform. In addition, the natural periods of the combined concept are also recorded. The natural periods in heave, roll, and pitch of the combined concept are significantly smaller than those of the FOWT system, because the additional damping effect provided by the tori increases the restoring force.

5.2. Power performance analysis of the combined system

5.2.1. Coupled motion between platform and WECs

This subsection analyzes the coupled motion of the combined concept in the rated condition (LC-3). One needs to note that the PTO in WEC combines a spring coefficient K_{PTO} = 10 kN/m and a damping coefficient B_{PTO} = 8000 kN·s/m. See Section 5.2.2 for a discussion on the selection of these two parameters.

As mentioned above, the tori can only slide in the direction of the column under limiters, so the power production of the WEC system is mainly affected by the relative heave motion between the tori and the platform. Fig. 3a shows the heave motion of the semi-submersible platform and the tori of WECs. Generally, the motions of the tori are significantly larger than the platform. The slight phase discrepancies between the torus 1, 2, and 3 with the platform are caused by the components of their different distances from the platform in the *x*-direction. The largest heave motion occurs on torus 1, which is determined by combining its maximum distance to the central column in the *x*-direction and the unique position at the wave-facing side. Fig. 3a,b show the relative motion and the relative velocity between the tori and the platform, respectively. Similar to Fig. 3a, the relative heave motion of torus 1 is the largest, which means that WEC 1 contributes the most to the wave energy production system when the damping coefficients of all WECs are the same. Fig. 3d compares the power output of the IEA 15 MW FOWT and the combined concept, respectively. It can be observed that the wind power fluctuates noticeably due to turbulent wind load, with an average value of about 14,162 kW below the rated power. Also, the output of the fixed turbine in rated turbulent wind load was recorded with an average value of 14.68 MW in 1 hour, which is better than that of the floating one. This phenomenon indicates that the pitch controller also contributes to the output fluctuations. Dramatic fluctuation in power output is significantly mitigated in other LCs. On the other hand, the similarity of the output of the two turbines illustrates the very limited effect of WECs on wind power.

5.2.2. Parameter study on PTO in WECs

In the present work, the PTO system in WEC can be simplified as a spring-damping model. The spring stiffness controls the motion synchronization between the torus and the platform, while the damping coefficient represents the energy absorption capacity of the WEC. Therefore, it is essential to choose a reasonable group of PTO coefficients. In this work, the spring stiffness is set to K_{PTO} = 10 kN/m following Muliawan et al. (2013b). The damping coefficients can be compared and decided in B_{PTO} = 2000, 8000, and 12,000 kN·s/m (Cheng et al., 2019).

Fig. 4 exhibits the mean values and Standard Deviations (STDs) of 1-h wind and wave power output of the combined system in different LCs. It can be found that the overall power performance of the WEC system is the best with B_{PTO} = 8000 kN·s/m. In all cases, the wave power is mainly dominated by torus 1, which benefits from the large relative motion induced by the pitch motion of the platform. Since columns 2 and 3 are symmetrically distributed along the *x*-axis in the *o-xz* plane, the power from WEC 2 and 3 should theoretically exhibit strong consistency. However, the platform yaw motion induced by the rotor makes the two tori movements different, which is very obvious in high wind speed cases (e.g., LC-1, LC-2, and LC-3). In addition, the damping coefficient hardly affects the wind power performance because of the limited effect induced by the tori.

In summary, the combination of K_{PTO} = 10 kN/m and B_{PTO} = 8000 kN·s/m is used in the following studies. It is worth noting that the combined system does not meet the power performance in the rated case (LC-3), where the average power is about 94.4 % of the expected value. In the high wind speed cases (LC-4, LC-5, and LC-6), the output stabilizes around 15.6 MW, slightly higher than the rated value, see Fig. 4f. However, the overestimation and underestimation of the power output can be mitigated in steady-state wind, indicating that the mispredictions

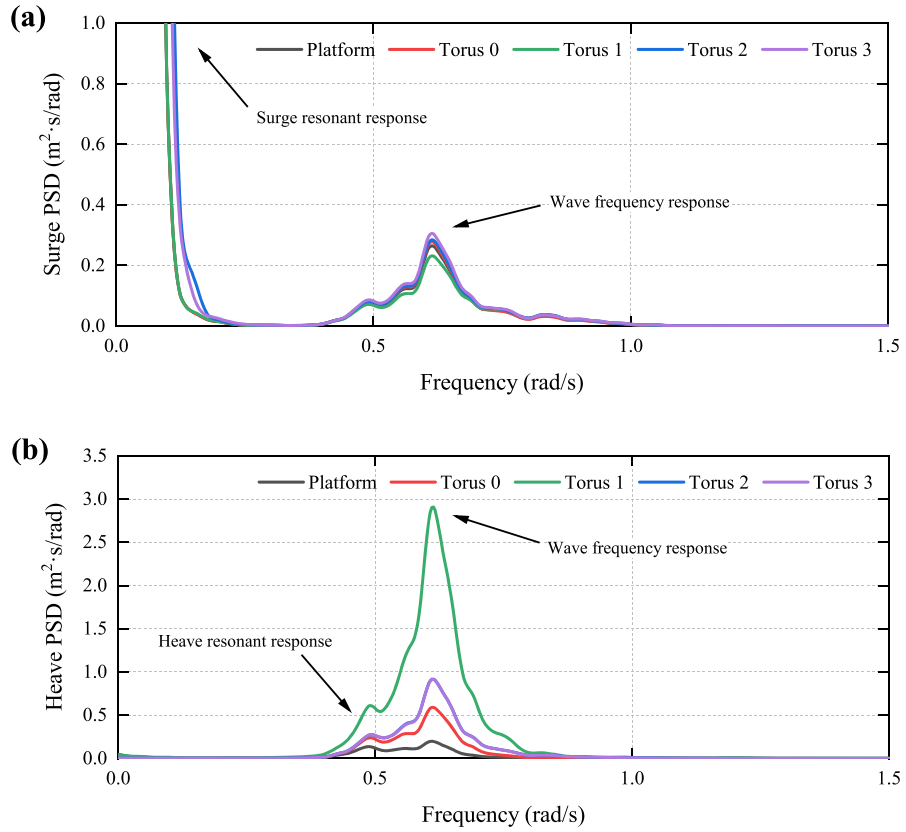

Fig. 8. Power spectra of surge and heave motions of the combined concept: (a) surge PSD and (b) heave PSD.

are caused by blade pitching.

5.2.3. Annual power production

Fig. 5a compares the mean values and STDs of the power output by the IEA 15 MW wind turbine and the combined system in all LCs. The wind power rises with increasing wind speed when the system is in the low wind speed cases (LC-1, LC-2, and LC-3), while the power is approximately constant with the controller in the high wind speed cases (LC-4, LC-5, and LC-6). For combined system, WECs further increase the mean power. Thus, the relatively high STDs in LC-4, LC-5, and LC-6 are caused by the drastically fluctuating WEC output.

Further, the mean values and STDs of the power of the wind turbine and WEC system in the combined system for all LCs are compared, as shown in Fig. 5b. The wind turbine capacity is significantly higher than the contribution of the WEC system. Meanwhile, the mean value and STD of WEC system power generation are mainly affected by wave height.

To objectively estimate the power performance of the combined concept in realistic environmental conditions, the annual power production of the turbine and the WECs were calculated separately and compared with the IEA 15 MW wind turbine, see Fig. 5c. In this work, it is assumed that the power generator operates throughout the year, so the annual power production can be roughly calculated from the annualized 1-h power production and the occurrence probability of the corresponding LC. The difference in annual power production between the two turbines is negligible, while the WECs could provide an additional 6.65 GW·h of power, about 11.4 % of the annual power production. This means that the power of the WEC system is approximately 0.75 MW. The annual wave power production is similar to the 6.3 GW·h for the combined system proposed by Li et al. (2022), which proves the effectiveness of the concept in this paper.

5.3. Dynamic analysis of the combined concept

5.3.1. Aerodynamic loads

For a FOWT system, the motion response of the overall structure and the wind power performance are dominated by the thrust and aerodynamic torque arising from the wind load, respectively. This means that we can assess the impact of WECs on dynamic performance by observing these two indexes.

The thrust and torque of the two systems are compared separately for all LCs, as shown in Fig. 6. It can be observed that the two turbines are in solid agreement in terms of mean thrust and mean torque. The difference is that the wind turbine blade pitch angle is readily tuned under the command of the controller against external loads to control the motion attitude. Thus, the thrust on the turbine is different. In addition, introducing tori leads to a more significant STD of the turbine thrust. However, tori do not significantly affect wind power production, which agrees with the conclusions drawn in Section 5.2.2.

5.3.2. Floater motions

Fig. 7a,b compare the surge and heave responses of the platform and torus 0 in the combined concept for all LCs. Since the torus is concentric with the platform initially and remains subject to the horizontal limiter, its surge motion is almost identical to the platform. For the heave motion, the mean values of the platform and torus are very close to 0 for all the cases, and the STDs keep growing with increasing wave height since bodies at the free surface are mainly affected by the waves.

The main factors contributing to the target response can be found based on power spectrum analysis. Hence, the surge and heave Power Spectral Density (PSD) of each device in LC-3 are shown in Fig. 8a,b for further analysis. Due to the mechanical constraint in the horizontal plane, the tori exhibit almost the same surge response spectra as the platform. Their surge spectra are dominated by surge resonance, wind load and wave load excitation. As for heave motion, the tori and

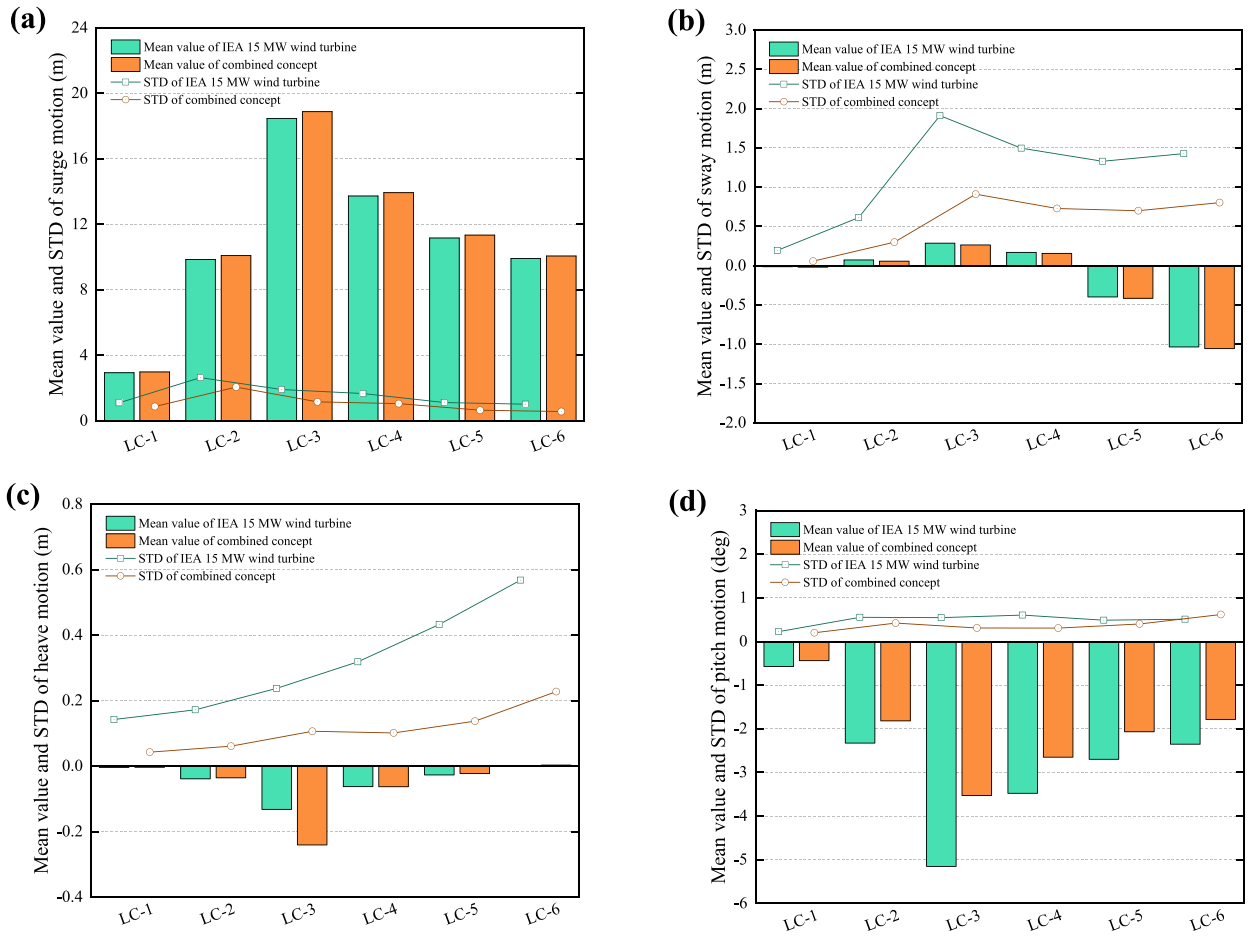

Fig. 9. Statistical comparisons of motions of the IEA 15 MW wind turbine and the combined concept: (a) surge motion, (b) sway motion, (c) heave motion, and (d) pitch motion.

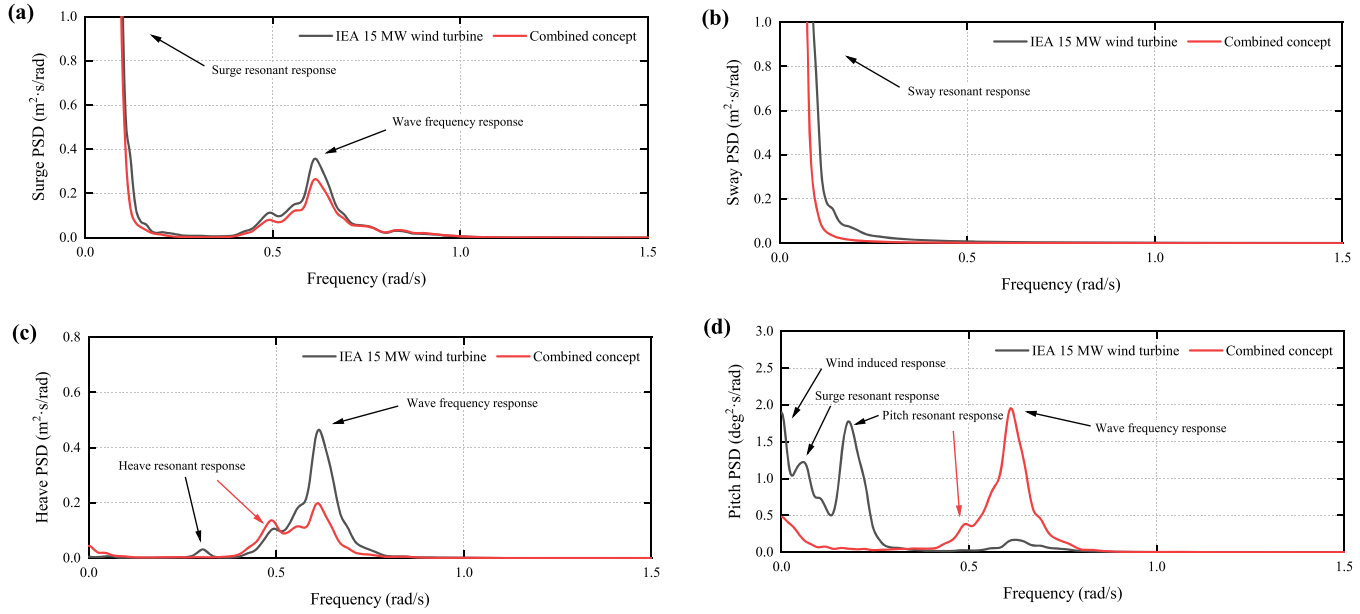

Fig. 10. Power spectra of motions of the IEA 15 MW wind turbine and the combined concept: (a) surge PSD, (b) sway PSD, (c) heave PSD, and (d) pitch PSD.

platform are primarily influenced by wave frequency response and their own heave resonance response. Meanwhile, the heave response of any torus under wave excitation is higher than that of the platform, which contributes to WEC power generation.

The effect of tori on the platform motion can be found by comparing the responses of the IEA 15 MW wind turbine and the combined concept.

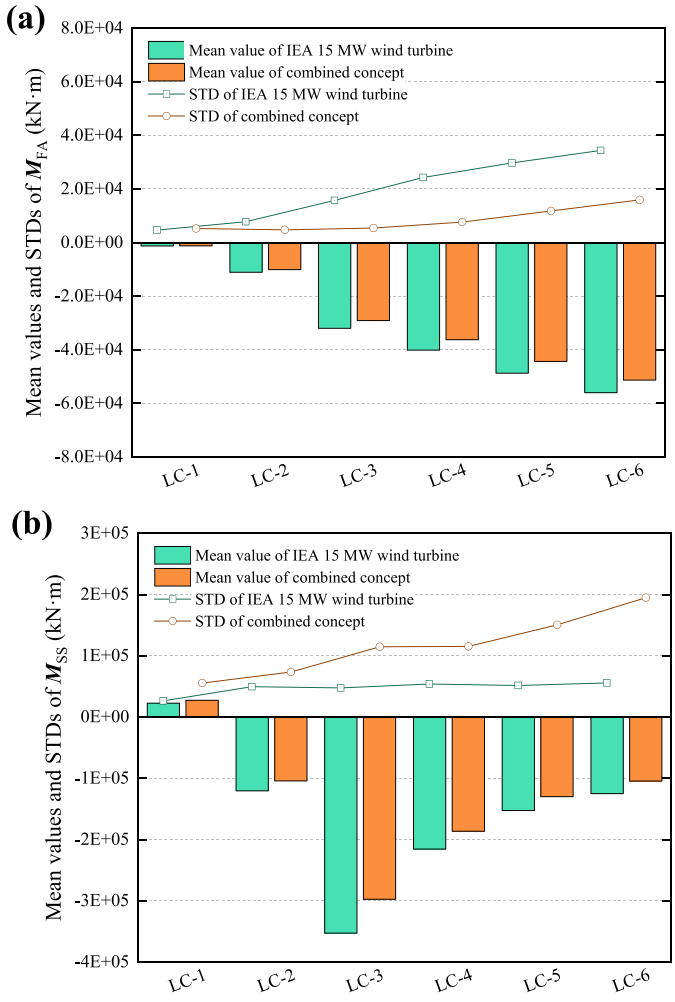

Fig. 11. Statistical comparisons of towing base bending moments of the IEA 15 MW wind turbine and the combined concept: (a) fore-aft bending moment and (b) side-side bending moment.

Fig. 9 compare the mean values and STDs of the platform motion responses in surge, sway, heave, and pitch for the IEA 15 MW wind turbine and combined concept. It can be noticed that introducing tori decreases the STDs of the combined concept, especially in the sway and heave motion. Also, tori significantly mitigate the mean pitch response. In the rated operating condition, the pitch amplitude of the combined concept is 31.5 % less than that of the FOWT, which implies that the combined concept motion is more stable.

The motion power spectra of the two platforms are displayed in Fig. 10. The main discrepancy between the motion power spectra appears in the wave frequency range for surge, sway, and heave motions. The surge and heave motion of the combined concept is slightly smaller than the IEA 15 MW turbine. The low-frequency responses are due to turbulent wind load and second-order difference-frequency wave excitation forces. The combined concept has a relatively more significant second-order wave excitation force because of the presence of the tori. However, the low-frequency surge, sway, and pitch motions of the combined concept are, in contrast, smaller than that of the IEA 15 MW wind turbine. The reason is that the torus also contributes to the damping and helps mitigate the low-frequency motions. In addition, tori lead to a larger pitch resonance frequency and make the system more sensitive to first-order wave excitations. In terms of heave motion, although the structural natural frequency is within the wave frequency range, it does not excite the wave frequency peak value, so the hybrid power generation system can still maintain stable motion. Note that the above analysis of the motion response does not consider the hydrodynamic coupling effect between the platform and the tori and thus may exit some deviation from reality.

5.3.3. *Tower base bending moment*

The tower base bending moment is mainly induced by the aerodynamic loads on the blades, the weight of rotor and nacelle, and the wave excitation forces on the platform. Thus, it is one of the most important indexes for estimating the dynamic response of the FOWT. This subsection compares the tower base fore-aft and side-side bending moments for the IEA 15 MW wind turbine and the combined concept.

Fig. 11 shows the statistics of the fore-aft and side-side bending moments for all LCs, respectively. It can be observed that the mean values and STDs of the tower base fore-aft bending moments for the combined concept are lower than those of the IEA 15 MW turbine, which is related to the reduction in the mean pitch motion of the platform induced by tori. For these two systems, the fore-aft bending moment grows with increasing wave height. Moreover, although the combined concept exhibits smaller mean values for side-side bending moments, it also amplifies the bending moment dispersion. The large mean values of side-side bending moment in LC-3 for both systems are caused by the thrust, see Fig. 6a.

Fig. 12 compares the power spectra of the tower base bending moments for the two systems. As shown in Fig. 12a, the violent turbulent wind load induces the pitch motion, and therefore, the fore-aft bending moment of the IEA 15 MW wind turbine is mainly dominated by wind. For the combined concept, the additional damping provided by tori effectively reduces this pitch motion. Unlike the IEA 15 MW wind turbine, the 1P aerodynamic pulse hardly contributes to the bending moment. As a result, the fore-aft bending moment of the combined concept is dominated by turbulent wind load, wave loads, and weak 3P aerodynamic loads. The side-side bending moment of the combined concept is dominated by waves and wind, as shown in Fig. 12b. In summary, the torus structure helps to reduce the pitch response of the system but also excites the sensitivity to waves to some extent.

5.3.4. *Mooring line tension*

The semi-submersible platform is connected to the seabed by a mooring system consisting of three R3 studless steel chain catenary to increase the yaw stiffness. Line 1 holds the most enormous mooring tension since it is parallel to the direction of wind-wave loads. Therefore, only the results of mooring line 1 are shown in this paper.

The mooring tension statistics of line 1 in all LCs are shown in Fig. 13a. The difference in the mean values of mooring tension between the combined concept and the IEA 15 MW turbine can be neglected. Overall, the mooring tensions for the IEA 15 MW turbine and the combined concept remain highly consistent, indicating that tori have a very limited effect on the mooring dynamics. In LC-3, the mooring tension is largest because both the surge and pitch motions of the platform are maximum at this time (Fig. 9a,b). For low wind speed cases, the mooring tension grows significantly with the increase of load intensity. In contrast, when the rated case is exceeded, the tension is inversely related to the load intensity and tends to stabilize with the controller. It shows a difference with (Li et al., 2022) because the mooring dynamics of the 15 MW wind turbine mainly result from the wind load, and the control strategy leads to a reduction in thrust. From the power spectra in Fig. 13b, it can be noticed that the tori increase the contribution of wave excitation to the mooring tension, as expected.

6. Conclusions

This work presents a novel wind-wave energy combined concept consisting of the IEA 15 MW wind turbine, the VolturnUS-S semi-submersible platform, and four torus-type point-absorber WECs. The FOWT system shares the platform, mooring system, and power cables with the WECs. The PTO system generates power by capturing the relative

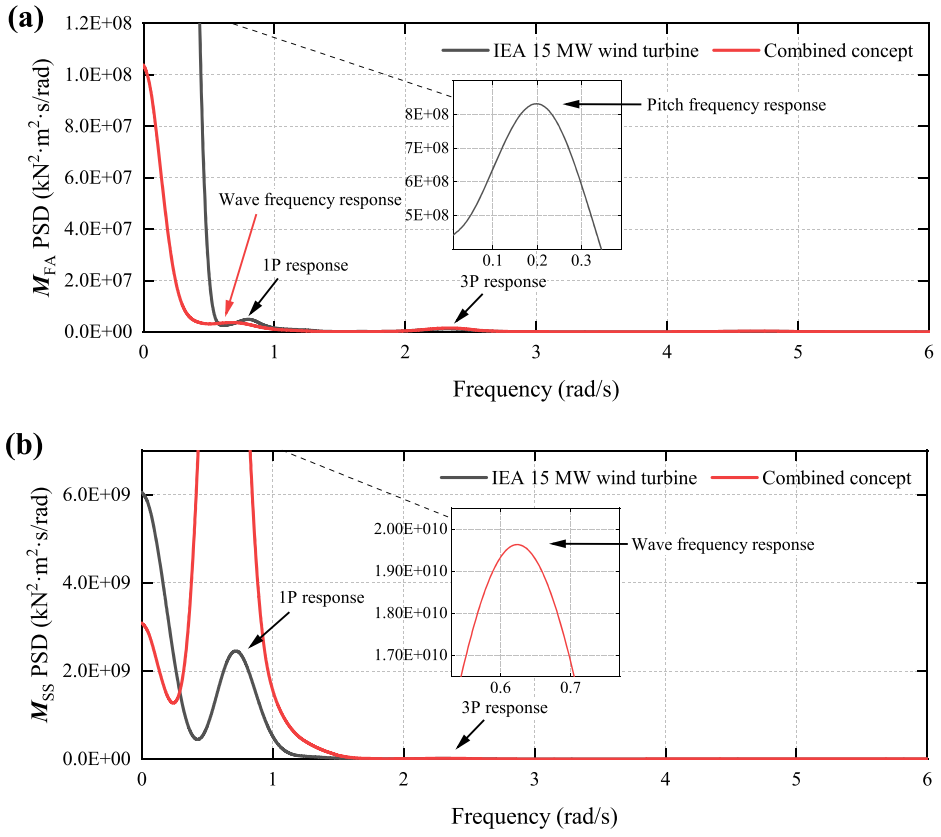

Fig. 12. Power spectra of towing base bending moments of the IEA 15 MW wind turbine and the combined concept: (a) fore-aft bending moment and (b) side-side bending moment.

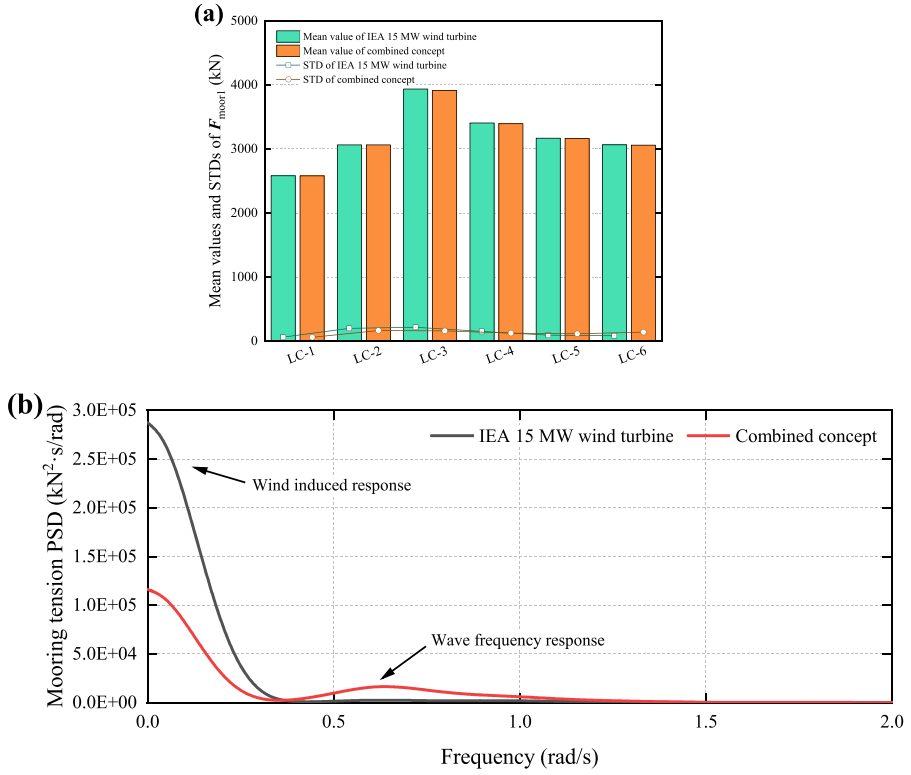

Fig. 13. Statistical comparisons and power spectra of mooring tension of the IEA 15 MW wind turbine and the combined concept: (a) Mean values and STDs and (b) power spectra of mooring tension.

motion between the platform and each torus, which is constrained by mechanical limiters. The coupled simulation of the FOWT is performed based on a time-domain numerical framework, SIMO-RIFLEX. The power performance and dynamic response of the combined concept in several irregular waves and turbulent wind load combinations are compared with the IEA 15 MW FOWT. The main conclusions of this work are summarized below:

i) For the combined concept, introducing tori would have little impact on wind energy capture. Following preliminary statistics, the total annual power production of the combined concept is about 58.2 GW·h, of which wave energy accounts for about 11.4 %. Thus, the power of the WEC system is approximately 0.75 MW.
ii) WEC 1 contributes the most to the wave energy generation system. The reason is that the distance between torus 1 and the central column has the longest projection on the *x*-axis, and the pitch motion induced by turbulent wind load leads to a more distinctive relative motion of torus 1 than the other tori. Another important point is that torus 1 is on the wave-facing side and is subjected to the direct impact of waves with less energy dissipation.
iii) The damping effects and storing moments from tori mitigate the platform's violent motion and significantly reduce the mean response in pitch. Under the rated condition, the pitch for the combined concept is reduced by 31.5 % compared to the FOWT, enhancing the platform's stability. Furthermore, the tori hardly have any impact on the aerodynamic loads.
iv) Based on previous research and the comparisons in this work, the combination of K_{PTO} = 10 kN/m and B_{PTO} = 8000 kN·s/m is selected for the WECs, as this combination performs well both in terms of individual WEC and total power output.
v) Compared to the IEA 15 MW FOWT, the tower base bending moment of the combined concept presents a weaker sensitivity to wind load. For the fore-aft bending moment, wind load still dominates, while the side-side bending moment is mainly influenced by waves. The combined concept has similar mooring dynamics properties with the IEA 15 MW turbine.

In summary, this paper provides a detailed study of the power performance and dynamic response of the proposed novel wind-wave energy power combination concept. The results show that the combined concept has great development potential due to its stable power output. However, only the performance of the concept in working conditions is considered, ignoring the case where the torus-shape WECs lock up in extreme states. In addition, the effects of hydrodynamic coupling between the platform and the torus should be considered for more accurate results. Further research on these issues will be conducted in the future.

CRediT authorship contribution statement

Xun Gu: Supervision, Investigation, Formal analysis, Methodology, Writing – original draft. **Fei Lin:** Writing – review & editing, Supervision, Conceptualization. **Wei Jiang:** Writing – review & editing, Supervision, Conceptualization. **Jie Xu:** Writing – review & editing, Supervision, Conceptualization. **Jia-Ming Liu:** Writing – original draft, Visualization, Validation, Software, Methodology, Data curation. **Kai Wang:** Writing – review & editing, Supervision, Project administration, Methodology, Investigation, Formal analysis, Conceptualization. **Tao Tao:** Writing – review & editing, Supervision, Resources, Investigation, Conceptualization.

Declaration of interests

The authors declare that they have no known competing financial interests or personal relationships that could have appeared to influence the work reported in this paper.

Acknowledgements

This work was supported by the Key technology research and demonstration project of 10 MW deep-sea floating offshore wind turbine (DTGD-2023–10174) - Key technology research task of floating offshore combined wind and wave power generation, Guangdong Basic and Applied Basic Research Foundation, China (Grant No. 2022B1515250005), and the National Natural Science Foundation of China (Grant No. 52171289).

The authors would also like to thank Yuefeng Chu from the School of Ocean Engineering and Technology, Sun Yat-sen University, for his technical support and advice on this work.

References

Allen, C.K., Viscelli, A., Dagher, H.J., Goupee, A.J., Gaertner, E., Abbas, N.J., Hall, M., Barter, G.E., 2020. Definition of the UMaine VolturnUS-S reference platform developed for the IEA wind 15-Megawatt offshore reference wind turbine, https://doi.org/10.2172/1660012.

Astariz, S., Iglesias, G., 2016. Selecting optimum locations for co-located wave and wind energy farms. Part I: the Co-Location Feasibility index. Energy Convers. Manage. 122, 589–598. https://doi.org/10.1016/j.enconman.2016.05.079.

Aubault, A., Alves, M., Sarmento, A., Roddier, D., Peiffer, A., 2011. Modeling of an oscillating water column on the floating foundation WindFloat. In: Proceedings of the ASME 2011 30th International Conference on Ocean, Offshore and Arctic Engineering, Volume 5: Ocean Space Utilization; Ocean Renewable Energy. Rotterdam, The Netherlands. ASME, pp. 235–246. https://doi.org/10.1115/OMAE2011-49014. June 19–24, 2011.

Bak, C., Zahle, F., Bitsche, R.D., Kim, T., Yde, A., Henriksen, L.C., Hansen, M.H., Blasques, J.P., Gaunaa, M., Natarajan, A., 2013. The DTU 10-MW reference wind turbine. Sound/Visual production (digital). Danish Wind Power Research 2013, Fredericia, Denmark, 27/05/2013.

Cheng, Z., Wang, K., Gao, Z., Moan, T., 2017. A comparative study on dynamic responses of spar-type floating horizontal and vertical axis wind turbines. Wind Energ 20, 305–323. https://doi.org/10.1002/we.2007.

Cheng, Z., Wen, T.R., Ong, M.C., Wang, K., 2019. Power performance and dynamic responses of a combined floating vertical axis wind turbine and wave energy converter concept. Energy 171, 190–204. https://doi.org/10.1016/j.energy.2018.12.157.

Creech, A., Früh, W.G., Maguire, A.E., 2015. Simulations of an offshore wind farm using large-eddy simulation and a torque-controlled actuator disc model. Surv. Geophys. 36, 427–481. https://doi.org/10.1007/s10712-015-9313-7.

Gaertner, E., Rinker, J., Sethuraman, L., Zahle, F., Anderson, B., Barter, G., Abbas, N., Meng, F., Bortolotti, P., Skrzypinski, W., Scott, G., Feil, R., Bredmose, H., Dykes, K., Shields, M., Allen, C., Viselli, A., 2020. Definition of the IEA 15-Megawatt Offshore Reference Wind Turbine. National Renewable Energy Laboratory (NREL). https://doi.org/10.2172/1603478.

Global Wind Energy Council (GWEC), 2024. Global wind report 2024.

Hegseth, J.M., Bachynski, E.E., Martins, J.R.R.A., 2020. Integrated design optimization of spar floating wind turbines. Mar. Struct. 72, 102771. https://doi.org/10.1016/j.marstruc.2020.102771.

Hu, J., Zhou, B., Vogel, C., Liu, P., Willden, R., Sun, K., Zang, J., Geng, J., Jin, P., Cui, L., Jiang, B., Collu, M., 2020. Optimal design and performance analysis of a hybrid system combing a floating wind platform and wave energy converters. Appl. Energy 269, 114998. https://doi.org/10.1016/j.apenergy.2020.114998.

IEA-15-240-RWT, 2024. https://github.com/IEAWindTask37/IEA-15-240-RWT/tree/master/OpenFAST/IEA-15-240-RWT-UMaineSemi (accessed July 8, 2024).

International Electrotechnical Commission (IEC), 2005. International Standard 61400-1, wind turbines, Part 1: design requirements.

Johannessen, K., Meling, T.S., Haver, S., 2002. Joint distribution for wind and waves in the northern North Sea. Int. J. Offshore Polar Eng. 12 (01).

Jonkman, B.J., 2009. Turbsim user's guide: version 1.50. United States. https://doi.org/10.2172/965520.

Kamarlouei, M., Gaspar, J.F., Calvario, M., Hallak, T.S., Mendes, M.J.G.C., Thiebaut, F., Guedes Soares, C., 2020. Experimental analysis of wave energy converters concentrically attached on a floating offshore platform. Renew. Energy 152, 1171–1185. https://doi.org/10.1016/j.renene.2020.01.078.

Li, J., Shi, W., Zhang, L., Michailides, C., Li, X., 2021. Wind-wave coupling effect on the dynamic response of a combined wind–wave energy converter. J Mar. Sci. Eng. 9 (10), 1101. https://doi.org/10.3390/jmse9101101.

Li, Y., Ong, M.C., Wang, K., Li, L., Cheng, Z., 2022. Power performance and dynamic responses of an integrated system with a semi-submersible wind turbine and four torus-shaped wave energy converters. Ocean Eng. 259, 111810. https://doi.org/10.1016/j.oceaneng.2022.111810.

Luan, C., Gao, Z., Moan, T., 2016. Design and analysis of a braceless steel 5-mw semi-submersible wind turbine. In: Proceedings of the ASME 2016 35th International Conference on Ocean, Offshore and Arctic Engineering, Volume 6: Ocean Space Utilization; Ocean Renewable Energy. Busan, South Korea. ASME. https://doi.org/10.1115/OMAE2016-54848. June 19–24, 2016. V006T09A052.

MARINA Platform, 2014. http://msp-platform.eu/projects/marina-platform (accessed July 8, 2024).

Michailides, C., Gao, Z., Moan, T., 2016a. Experimental and numerical study of the response of the offshore combined wind/wave energy concept SFC in extreme environmental conditions. Mar. Struct. 50, 35–54. https://doi.org/10.1016/j.marstruc.2016.06.005.
Michailides, C., Gao, Z., Moan, T., 2016b. Experimental study of the functionality of a semisubmersible wind turbine combined with flap-type wave energy converters. Renew. Energy 93, 675–690. https://doi.org/10.1016/j.renene.2016.03.024.
Muliawan, M.J., Gao, Z., Moan, T., Babarit, A., 2011. Analysis of a two-body floating wave energy converter with particular focus on the effects of power take-off and mooring systems on energy capture. In: Proceedings of the ASME 2011 30th International Conference on Ocean, Offshore and Arctic Engineering. Volume 5: Ocean Space Utilization; Ocean Renewable Energy. Rotterdam, The Netherlands. ASME, pp. 317–328. https://doi.org/10.1115/OMAE2011-49135. June 19–24, 2011.
Muliawan, M.J., Karimirad, M., Moan, T., Gao, Z., 2012. STC (spar-torus combination): a combined spar-type floating wind turbine and large point absorber floating wave energy converter-promising and challenging. In: Proceedings of the ASME 2012 31st International Conference on Ocean, Offshore and Arctic Engineering. Volume 7: Ocean Space Utilization; Ocean Renewable Energy. Rio de Janeiro, Brazil. ASME, pp. 667–676. https://doi.org/10.1115/OMAE2012-84272. July 1–6, 2012.
Muliawan, M.J., Karimirad, M., Gao, Z., Moan, T., 2013a. Extreme responses of a combined spar-type floating wind turbine and floating wave energy converter (STC) system with survival modes. Ocean Eng. 65, 71–82. https://doi.org/10.1016/j.oceaneng.2013.03.002.
Muliawan, M.J., Karimirad, M., Moan, T., 2013b. Dynamic response and power performance of a combined spar-type floating wind turbine and coaxial floating wave energy converter. Renew. Energy 50, 47–57. https://doi.org/10.1016/j.renene.2012.05.025.
Musial, W., Butterfield, S., Ram, B., 2006. Energy from offshore wind: preprint. United States. https://doi.org/10.4043/18355-MS.
Namik, H., Stol, K., 2014. Individual blade pitch control of a spar-buoy floating wind turbine. IEEE Trans. Control Syst. Technol. 22 (1), 214–223. https://doi.org/10.1109/TCST.2013.2251636. Jan. 2014.
Peiffer, A., Roddier, D., Aubault, A., 2011. Design of a point absorber inside the WindFloat structure. In: Proceedings of the ASME 2011 30th International Conference on Ocean, Offshore and Arctic Engineering. Volume 5: Ocean Space Utilization; Ocean Renewable Energy. Rotterdam, The Netherlands. ASME, pp. 247–255. https://doi.org/10.1115/OMAE2011-49015. June 19–24, 2011.
Peiffer, A., Roddier, D., 2012. Design of an oscillating wave surge converter on the WindFloat* structure. In: 4th International Conference on Ocean Energy. Dublin. October 17, 2012.
Ren, N., Gao, Z., Moan, T., 2014. Long-term stochastic dynamic analysis of a combined floating spar-type wind turbine and wave energy converter (STC) system for mooring fatigue damage and power prediction. In: Proceedings of the ASME 2014 33rd International Conference on. San Francisco, California, USA. Ocean, Offshore and Arctic Engineering. Volume 9A: Ocean Renewable EnergyASME. https://doi.org/10.1115/OMAE2014-23438. June 8–13, 2014. V09AT09A026.
Ren, N., Gao, Z., Moan, T., Wan, L., 2015. Long-term performance estimation of the Spar-Torus-Combination (STC) system with different survival modes. Ocean Eng. 108, 716–728. https://doi.org/10.1016/j.oceaneng.2015.08.013.
Ren, N., Ma, Z., Shan, B., Ning, D., Ou, J., 2020. Experimental and numerical study of dynamic responses of a new combined TLP type floating wind turbine and a wave energy converter under operational conditions. Renew. Energy 151, 966–974. https://doi.org/10.1016/j.renene.2019.11.095.
Si, Y., Chen, Z., Zeng, W., Sun, J., Zhang, D., Ma, X., Qian, P., 2021. The influence of power-take-off control on the dynamic response and power output of combined semi-submersible floating wind turbine and point-absorber wave energy converters. Ocean Eng. 227, 108835. https://doi.org/10.1016/j.oceaneng.2021.108835.
Si, Y., Karimi, H.R., Gao, H., 2014. Modelling and optimization of a passive structural control design for a spar-type floating wind turbine. Eng. Struct. 69, 168–182. https://doi.org/10.1016/j.engstruct.2014.03.011.
Sun, K., Yi, Y., Zheng, X., Cui, L., Zhao, C., Liu, M., Rao, X., 2021. Experimental investigation of semi-submersible platform combined with point-absorber array. Energy Convers. Manage. 245, 114623. https://doi.org/10.1016/j.enconman.2021.114623.
Tian, W., Wang, Y., Shi, W., Michailides, C., Wan, L., Chen, M., 2023. Numerical study of hydrodynamic responses for a combined concept of semisubmersible wind turbine and different layouts of a wave energy converter. Ocean Eng. 272, 113824. https://doi.org/10.1016/j.oceaneng.2023.113824.
Wan, L., Gao, Z., Moan, T., 2014. Model test of the STC concept in survival modes. In: Proceedings of the ASME 2014 33rd International Conference on Ocean, Offshore and Arctic Engineering. Volume 9A: Ocean Renewable Energy. San Francisco, California, USA. ASME. https://doi.org/10.1115/OMAE2014-23213. June 8–13, 2014. V09AT09A010.
Wan, L., Gao, Z., Moan, T., 2015. Experimental and numerical study of hydrodynamic responses of a combined wind and wave energy converter concept in survival modes. Coast. Eng. 104, 151–169. https://doi.org/10.1016/j.coastaleng.2015.07.001.
Wan, L., Gao, Z., Moan, T., Lugni, C., 2016a. Comparative experimental study of the survivability of a combined wind and wave energy converter in two testing facilities. Ocean Eng. 111, 82–94. https://doi.org/10.1016/j.oceaneng.2015.10.045.
Wan, L., Gao, Z., Moan, T., Lugni, C., 2016b. Experimental and numerical comparisons of hydrodynamic responses for a combined wind and wave energy converter concept under operational conditions. Renew. Energy 93, 87–100. https://doi.org/10.1016/j.renene.2016.01.087.
Xu, K., Larsen, K., Shao, Y., Zhang, M., Gao, Z., Moan, T., 2021a. Design and comparative analysis of alternative mooring systems for floating wind turbines in shallow water with emphasis on ultimate limit state design. Ocean Eng. 219, 108377. https://doi.org/10.1016/j.oceaneng.2020.108377.
Xu, S., Murai, M., Wang, X., Takahashi, K., 2021b. A novel conceptual design of a dynamically positioned floating wind turbine[J]. Ocean Eng. 221, 108528. https://doi.org/10.1016/j.oceaneng.2020.108528.
Yang, Y., Bashir, M., Wang, J., Yu, J., Li, C., 2020. Performance evaluation of an integrated floating energy system based on coupled analysis. Energy Convers. Manage. 223, 113308. https://doi.org/10.1016/j.enconman.2020.113308.
Zahle, F., Barlas, A., Lønbæk, K., Bortolotti, P., Zalkind, D., Wang, L., Labuschagne, C., Sethuraman, L., Barter, G., 2024. Definition of the IEA Wind 22-Megawatt Offshore Reference Wind Turbine. Technical University of Denmark. https://doi.org/10.11581/DTU.00000317.
Zhang, D., Chen, Z., Liu, X., Sun, J., Yu, H., Zeng, W., Ying, Y., Sun, Y., Cui, L., Yang, S., Qian, P., Si, Y., 2022. A coupled numerical framework for hybrid floating offshore wind turbine and oscillating water column wave energy converters. Energy Convers. Manage. 267, 115933. https://doi.org/10.1016/j.enconman.2022.115933.
Zhou, B., Hu, J., Jin, P., Sun, K., Li, Y., Ning, D., 2023. Power performance and motion response of a floating wind platform and multiple heaving wave energy converters hybrid system. Energy 265, 126314. https://doi.org/10.1016/j.energy.2022.126314.

Xun Gu is an engineer at Guangdong Datang International Chaozhou Power Generation Co., Ltd. He received bachelor's degree from Shenyang Institute of Engineering. His research interests include offshore wind power, electrical engineering, and new energy planning and development.

Fei Lin is an engineer at China Datang Corporation Ltd. Guangdong Branch. She received bachelor's degree from Northeast Electric Power University. Her research interests include new energy and thermal power innovation technologies.

Wei Jiang is a senior engineer at China Datang Corporation Ltd. Guangdong Branch. He received Ph.D. from University of Science and Technology of China. His research interests include renewable energy generation and new energy storage.

Jie Xu is an engineer at Guangdong Datang International Chaozhou Power Generation Co., Ltd. He received bachelor's degree from North China Electric Power University. His research interests include renewable energy and wave power generation.

Jia-Ming Liu is an Ph.D. candidate at Sun Yat-sen University (SYSU). He is interested in floating offshore wind turbines and wind-fishery integration systems.

Kai Wang* is an associate professor at Sun Yat-sen University (SYSU). He received Ph.D. from Norwegian University of Science and Technology (NTNU). His research interests include the fully coupled simulation of novel floating wind turbines, combined wind-wave energy utilization devices, and wind-fishery integration devices.

Tao Tao is an engineer at China Southern Power Grid Technology Co, Ltd. He received Ph.D. from North China Electric Power University. His research interests include modeling and simulation, condition monitoring and fault diagnosis of offshore wind turbines and wave energy generation devices.